Bulletin of Geophysics and Oceanography Vol. 67, n. 3, pp. 439-460; September 2026
DOI 10.4430/bgo00527

Machine learning-based automated horizontal-to-vertical spectral ratio analysis for site characterisation and regional transferability using KiK-net data in the Kathmandu Valley

D. Poudyal Lohani

Department of Civil Engineering, Nepal Engineering College, Changunarayan, Bhaktapur, Nepal

(Received: 7 October 2025; accepted: 9 February 2026; published online: 20 August 2026)

ABSTRACT The Kathmandu Valley faces high seismic risk due to its Himalayan location and thick sediments. Traditional horizontal-to-vertical spectral ratio (HVSR) analysis relies on manual interpretation, limiting scalability. This study introduces automated HVSR, a machine learning (ML) framework automating HVSR processing for site characterisation. Using a comprehensive dataset of 2,363 earthquakes from the Kiban Kynoshin network (KiK-net), a strong-motion network in Japan, three ML models were used to predict the dominant frequency (f_d) from HVSR curves, namely: random forest, support vector regression (SVR) with a linear kernel, and SVR with a radial basis function kernel. The linear SVR model demonstrated an R^2 value of 0.992, root mean square error of 1.54, and mean absolute error of 1.397 Hz. Bootstrap uncertainty analysis showed narrow confidence ranges for most samples, confirming stable and consistent predictions. Feature importance results indicate that the f_d and mean frequency carry nearly all predictive weights, while amplitude-based parameters contribute very little. A feature space overlap assessment further demonstrated that the f_d and amplification ranges in the KiK-net dataset align well with expected site response characteristics of the Kathmandu Valley. The workflow offers a practical and scalable solution for data scarce regions and provides a strong foundation for future microzonation and site response studies.

Key words: feature importance, HVSR, KiK-net, overlap assessment, random forest, support vector regression, ridge regression, uncertainty analysis.

1. Introduction

Seismology is a critical field of study that aims to understand and mitigate the risk associated with earthquakes, particularly in urban areas prone to seismic activity. Among the various techniques employed in seismic analysis, the horizontal-to-vertical spectral ratio (HVSR) method stands out for its effectiveness in assessing site effects and seismic vulnerabilities. Nakamura (1989) proposed a novel approach for assessing the dynamic properties of subsurface layers by analysing microtremors recorded solely at ground surface. The HVSR method is based on the principle that the ratio between the horizontal and vertical components of ambient or seismic vibrations reflects the natural resonance characteristics of the subsurface layers, enabling the estimation of the dominant frequency (f_d) of the sites. However, despite its popularity, traditional HVSR workflows still heavily rely on the manual interpretation of spectral curves, which is time consuming, subjective, and not scalable for large datasets or rapid hazard assessments (Xu and

Wang, 2021). Recent efforts have sought to overcome these limitations through automation. The pioneering automated HVSR (AutoHVSR) algorithm by the Vantassel *et al.* (2023) instance, integrated advanced signal processing and ML to automate the calculation of f_d and amplification, with high precision, achieving an accuracy of over 99% and root mean square error (RMSE) as low as 0.05 Hz, about 138 times faster than manual methods.

This aligns with a broader trend that integrates machine learning (ML) with HVSR analysis, as seen in Phi *et al.* (2024) who developed a seismic site classification prediction model by integrating ML techniques with the HVSR method, where the light gradient boosting machine combined with outlier detection and the synthetic minority oversampling technique achieved the highest accuracy of 0.91 and F1 score of 0.79. Similarly, Cai and Xi (2024) proposed a support vector machine (SVM) based site classification model using HVSR features and strong ground motion data from the Kiban Kyoshin network (KiK-net) and the Kyoshin network (K-NET) to reduce reliance on costly borehole data which achieved 76.12% accuracy with strong recall and precision across site classes, outperforming the spectral ratio and generalised regression neural network method. Furthermore, Wang *et al.* (2023) applied ML [random forest (RF), extreme gradient boosting (XGBoost), deep neural network] to predict site amplification from six key parameters using 353,327 KiK-net records. XGBoost performed best, and Shapley additive explanations analysis highlighted parameter importance, proving that ML outperforms traditional ground motion prediction equations for seismic hazard assessment. Instead, Zhu *et al.* (2023) compared a RF model with the traditional one dimensional ground response analysis (GRA) to predict site amplification. Using data from 1,580 sites for training and 145 for testing, the RF model, which incorporates parameters such as V_{S30}, peak frequency, and surface roughness, showed lower intersite variability and more effectively captured site specific characteristics, resulting in more reliable performance than the GRA approach. Globally, the HVSR method has been extensively applied to characterise site effects in diverse geological settings. Studies in regions like Semarang (Supriyadi *et al.*, 2022; Nurwidyanto *et al.*, 2023) and the Kalibening district (Saputra *et al.*, 2022) focused on the site effects and seismic vulnerability using the HVSR method to determine key parameters such as f_d, soil amplification, and the seismic vulnerability index, providing valuable models for regional seismic risk assessment. Lachet and Bard (1994) validated HVSR results with earthquake recordings, and Nogoshi and Igarashi (1971) contributed to the methodology by analysing soil response characteristics using microtremors. In the context of Nepal, Dhakal *et al.* (2016) analysed the HVSRs of S waves from aftershock data and found that the basin sediments significantly amplified the long period ground motion components generated by the mainshock and subsequent large aftershocks, while Pokhrel *et al.* (2019) used the HVSR technique to calculate the average shear wave velocity for the Kathmandu Valley. Similarly, Poudyal *et al.* (2024) conducted nonlinear (NL) ground response analysis to calculate the vulnerability index (0.22 to 21.84.) based on soil amplification (0.13 to 8.14.) and f_d (0.08 to 7.65 Hz). Poudyal *et al.* (2026) compared equivalent linear (EL) and NL site response analyses for the Kathmandu Valley using DEEPSOIL, borehole data, and ground motions from the 2015 Gorkha and 1995 Kobe earthquakes. Statistical analyses in MATLAB were used to examine the peak ground acceleration (*PGA*) and displacement relationship. The results show that the NL analysis better captures soil nonlinearity, with the Gorkha NL case indicating strong displacement reduction and more than 50% lower estimates than the EL, emphasising the importance of NL analysis for reliable seismic hazard assessment.

Tiwari *et al.* (2025) applied three ML models to predict earthquake magnitudes greater than 6 m_b in central Himalaya in 2015. Among them, the RF regressor demonstrated the best overall performance, achieving the lowest mean absolute error (*MAE*) of 0.36, mean square error

(*MSE*) of 0.23, and *RMSE* of 0.48, along with the highest accuracy (0.16), indicating its superior prediction capability. The support vector regression (SVR) followed closely, with a *MAE* of 0.35, *MSE* of 0.24, *RMSE* of 0.49, and an accuracy of 0.13. In contrast, the multilayer perceptron regressor performed the worst, yielding the highest error values with a MAE of 0.40, *MSE* of 0.27, and *RMSE* of 0.52, and the lowest accuracy at just 0.016. Similarly, Poudyal Lohani *et al.* (2025) evaluated seismic amplification in Bhaktapur by combining NL site response analysis (DEEPSOIL) for the 2015 Gorkha and 1995 Kobe earthquakes with ML [SVR, linear regression (LR), RF, ridge regression (RR)] to predict *PGA* and amplification ratio. Results show higher amplification in central and south-eastern areas, with LR and RF providing the most accurate predictions and RF showing the best generalisation.

The review by Poudyal *et al.* (2022, 2025a) emphasises the urgent need for seismic microzonation as a critical tool for earthquake risk mitigation, particularly for guiding authorities and policymakers. With increasing urbanisation and unregulated development, communities remain highly vulnerable to future earthquakes potentially more severe than the 2015 Gorkha event (Poudyal *et al.*, 2025c). Similarly, Poudyal *et al.* (2025b) conducted a topographic analysis of the Kathmandu Valley and found that areas with low topographic slopes, primarily in the central valley, exhibit higher soil amplification due to unconsolidated sediment deposits. Despite these efforts, a fully AutoHVSR ML framework for local site response analysis has not yet been implemented for Nepal.

To address these limitations, this study introduces enhanced AutoHVSR, a fully AutoHVSR analysis framework that integrates ML models, including RF, SVR, and RR. AutoHVSR estimates key site response parameters like f_d and the amplification factor, with minimal human intervention. Unlike traditional approaches, this automated framework improves reproducibility, enables rapid processing across large datasets, and enhances consistency in resonance peak identification. This study adapts and applies the AutoHVSR framework to data from the KiK-net strong motion network and extends its application to the Kathmandu Valley. This region, characterised by dense urbanisation, complex sedimentary layering, and limited strong motion data, presents an ideal test case for AutoHVSR workflows. By demonstrating the accuracy and scalability of AutoHVSR in this context, this research lays the foundation for data-driven seismic site characterisation that can enhance infrastructure resilience, urban planning, and earthquake disaster preparedness in the central Himalayas.

2. Methodology

2.1. Dataset and study area

The dataset utilised in this study is publicly accessible on the KiK-net website (National Research Institute for Earth Science and Disaster Resilience, n.d.). KiK-net is a prominent strong motion seismograph network operated by the National Research Institute for Earth Science and Disaster Resilience in Japan, consisting of 513 stations distributed across the country. This unique configuration provides valuable insights into seismic wave propagation through different geological layers. The dataset utilised in this study consists of 2,363 earthquakes recorded during the past years, more precisely from 2010 to 2025. While the ML models were trained and validated using KiK-net data from Japan, the broader aim of this study is to develop a robust, transferable framework, AutoHVSR, that can be applied to data scarce regions such as the Kathmandu Valley. This is especially relevant given the limited availability of local strong motion recordings in Nepal, combined with the complex geological setting and high seismic risk in the valley.

2.2. Data preprocessing and signal processing

The rich KiK-net dataset enables the development of reliable ML models, which can be fine-tuned in future work using local microtremor and geological data from the Kathmandu Valley.

This study employs a systematic approach that integrates HVSR analysis with ML techniques to assess seismic site characterisation. The workflow begins with the acquisition of seismic waveform data, consisting of time series measurements of ground motion in three directions: N-S, E-W, and vertical. Data preprocessing is performed to handle missing values, remove extreme outliers exceeding ±5 standard deviations (σ_s), and ensure proper scaling for ML applications. A fourth order low pass Butterworth filter with a cutoff frequency of 20 Hz is applied to the detrended signals to remove high frequency noise. The workflow of the proposed AutoHVSR framework, integrating HVSR computation and ML for f_d prediction, is illustrated in Fig. 1. The schematic diagram outlines the sequential process starting from data acquisition from the KiK-net, preprocessing and filtering, HVSR computation, feature extraction, and subsequent ML model training and evaluation.

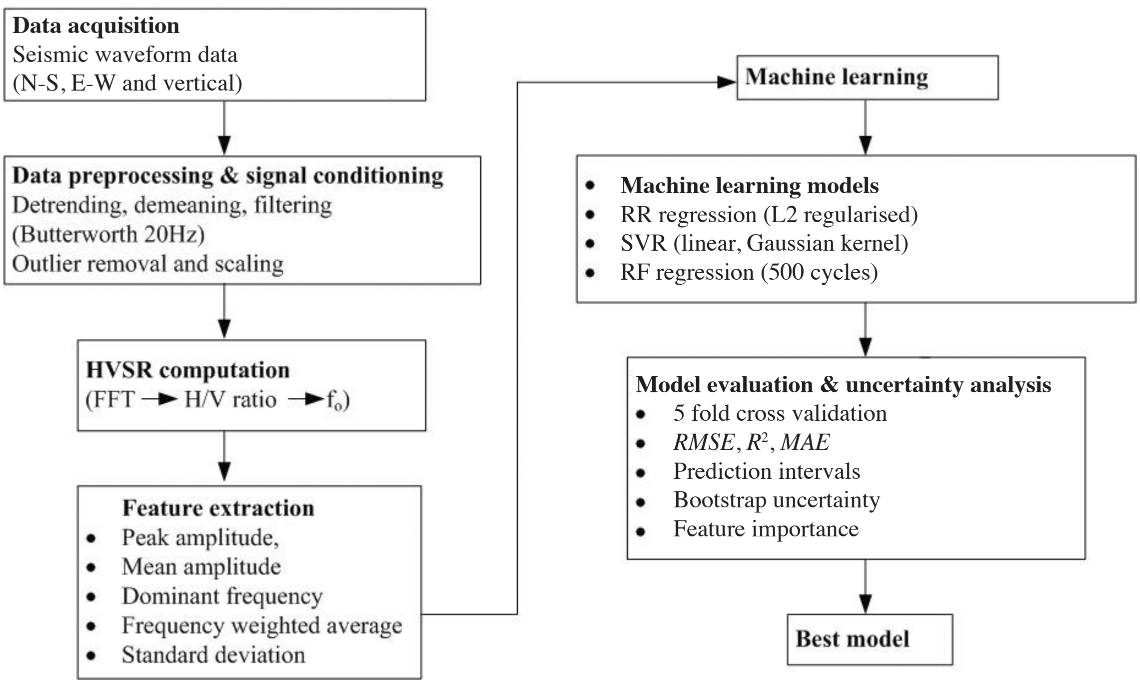

Fig. 1 - Methodological flowchart illustrating the AutoHVSR framework integrating HVSR computation and ML.

2.3. Horizontal-to-vertical spectral ratio computation

The horizontal seismic component (H) is calculated by combining the east and north components. First, the signals are standardised by dividing them by their respective σ_s. H is, then, computed [Eq. (1)] as the root sum of squares of the east and north components:

$$H = \frac{\sqrt{(North - South)^2 + (East - West)^2}}{\sqrt{2}} . \quad (1)$$

To determine the f_d, the fast Fourier transform (FFT) is applied to H, and the frequency with the highest spectral amplitude is identified. The f_d corresponds to the frequency at the peak of the power spectral density:

$$f_d = f_{peak}\,(P_H) \quad (2)$$

where P_H is the normalised horizontal spectrum.

The HVSR is calculated by dividing the horizontal spectrum by the vertical spectrum. The formula for the HVSR is:

$$\frac{H}{V} = \frac{P_H}{P_V} . \quad (3)$$

where, P_H and P_V are the positive half of the Fourier magnitude spectra of the horizontal and vertical components, respectively. The resulting HVSR curves were smoothed using a moving average filter to reduce noise while preserving essential spectral features. From each HVSR curve, five key features were extracted to serve as inputs for the ML models. These features are peak amplitude, f_d, mean amplitude, and frequency weighted average. The f_d served as the target variable for regression modelling.

2.4. Machine learning framework

Three supervised regression models were implemented to predict f_d extracted from HVSR results based on the engineered features:

1) RR (with automatic lambda selection using cross validation);
2) SVR method with linear and SVR method with linear, and radial basis function (RBF) (Gaussian kernel);
3) RF regression with 500 learning cycles.

Hyperparameter tuning was handled using MATLAB built in optimisation routines to ensure stable model performance. For RR, regularisation parameter λ was selected using five-fold internal cross validation. For SVR (linear and RBF), MATLAB automatic hyperparameter optimiser adjusted C, ε, and kernel scale parameter γ based on standardised features. For RF, bootstrap aggregation with 500 trees was used, where parameters such as split criteria and tree depth were optimised internally. These optimised values are not directly exposed to the user, because MATLAB computes them internally during training. Table 1 summarises the main hyperparameters and the optimisation strategy used for each model.

RR is a regularised linear regression model that incorporates L_2 regularisation to prevent

Table 1 - Hyperparameter configuration.

Model	Key parameters	Optimisation method	Configuration details
Ridge Regression (RR)	Regularisation coefficient (λ)	Five-fold cross validation	λ automatically selected by MATLAB (final value ≈ 0.008547)
SVR (linear)	C, ε	MATLAB automatic hyperparameter tuning	C and ε optimised with standardisation applied
SVR (RBF)	C, ε, γ	MATLAB automatic hyperparameter tuning	C and ε optimised with standardisation applied
Random Forest (RF)	Number of trees	Bootstrap aggregation (bagging)	500 trees with bootstrap sampling

overfitting. It minimises the residual sum of squares while adding a penalty proportional to the square of the magnitude of the coefficients. The model optimises the following cost function:

$$\min_{\beta}\left\{\sum_{i=1}^{n}(y_i - x_i\beta)^2 + \lambda\sum_{j=1}^{p}\beta_j^2\right\}$$

where, y_i is the actual f_d (Hz) for the i^{th} sample; x_i is the feature vector (x_{i1}, x_{i2}, x_{i3}, x_{i4}, x_{i5}) where x_{i1} is the peak amplitude HVSR, x_{i2} is the f_d, x_{i3} is the mean amplitude HVSR, x_{i4} is the σ of amplitudes, and x_{i5} is the frequency weighted average; β represents the model coefficients (β_1, β_2, β_3, β_4, β_5) representing the weight of each HVSR feature; λ is the regularisation parameter selected automatically using five-fold internal cross validation; n is the number of training samples; and p is the number of features (five HVSR parameters).

In the context of HVSR analysis, the RR model establishes the linear relationship between the five extracted HVSR features and the f_d. Coefficients β_1 through β_5 quantify how much each feature contributes to the f_d prediction. For instance, a high positive β_1 indicates that higher peak amplitudes strongly correlate with higher f_ds, while regularisation ensures that correlated features (like peak amplitude and mean amplitude) do not lead to unstable predictions.

SVR extends the principles of SVMs to regression tasks by finding a function that deviates from the actual values by no more than the tolerance parameter for each training point. A Gaussian kernel, also known as the RBF, transforms the input features into a higher dimensional space to effectively capture and model NL relationships.

The Gaussian kernel is expressed as:

$$K(x, x') = \exp(-\gamma||x - x'||^2) \quad (4)$$

where x and x′ represent pairs of feature vectors from the training dataset of 1,654 training samples. Here x is a feature vector in a five-dimensional space, namely: x=(x1,x2,x3,x4,x5) where: x1 represents the peak amplitude, x2 the peak frequency, x3 the mean amplitude, x4 the σ of amplitude, and x5 the frequency weighted average. ||x -x′|| is the Euclidean distance between the two feature vectors x=xi=(xi1,xi2,xi3,xi4,xi5) and x′=xj=(xj1,xj2,xj3,xj4,xj5) in the five-dimensional space; γ the Kernel scale parameter optimised during training. This kernel effectively measures the similarity between HVSR feature profiles, enabling the model to make predictions based on the f_ds of seismically similar sites in the training data.

RF regression, an ensemble learning method based on decision trees, was employed with 500 learning cycles to reduce overfitting and variance by averaging predictions across multiple decision trees. The prediction function of a RF model is given by:

$$y = \frac{1}{T}\sum_{t=1}^{T} f_t(x) \tag{5}$$

where T is the total number of trees (500), and f_t (x) represents the prediction of the t^{th} tree for input feature vector x; x is the input feature vector containing the five HVSR parameters; and y is the predicted f_d (Hz).

For HVSR analysis, each decision tree in the RF learns to split the data based on the threshold values of the five features. For example, a tree might first split sites based on whether their peak amplitude exceeds 2.5, and, then, further split based on frequency weighted average being above or below 1.2 Hz. The ensemble of 500 such diverse trees captures complex NL relationships between HVSR curve characteristics and f_d that would be difficult to model with single parametric equations.

Each tree is trained on a bootstrapped subset of the training data, with feature selection performed at each node to reduce correlation between trees. The final output is calculated by taking the average of the predictions made by all individual trees in the ensemble. RF regression is highly robust against overfitting and works well with both linear and NL data distributions, making it suitable for seismic vulnerability prediction. A five-fold cross validation strategy was adopted to evaluate performance, ensuring that each observation was used for training and testing exactly once. The training dataset (70% of total data, approximately 1,654 samples) was randomly partitioned into five equal-sized subsets or folds, each containing approximately 331 samples. During each iteration of the cross validation process, four folds (approximately 1,324 samples) were used for model training, while the remaining single fold (approximately 331 samples) served as the validation set.

The cross validation process specifically addressed the fundamental challenge in the HVSR-based prediction ensuring that models generalise to new seismic sites not seen during training. The iterative rotation of different validation subsets demonstrates that the extracted relationships maintain robustness across varying geographic distributions and are not biased towards specific earthquake events in the Japanese dataset. This procedure was repeated five times, with each fold serving exactly once as the validation set, ensuring that every observation in the training data was used for both training and validation. The cross validation process served multiple critical purposes: 1) hyperparameter optimisation for each algorithm, including λ in RR, γ in SVR RBF, and tree depth in RF; 2) model selection by comparing average performance across folds; and 3) variance reduction in performance estimates by providing five different train validation splits. Following cross validation on the training set, the best performing model configurations were retrained on the entire training dataset and evaluated on the completely held out test set (30% of total data, approximately 709 samples) that had no involvement in the cross validation process. Beyond standard *RMSE* and R^2 metrics, the *MAE* was computed to provide a multi-faceted performance assessment. Uncertainty quantification was performed through three complementary approaches: 1) Residual-based prediction intervals derived using the independent test dataset. The residuals between observed and predicted f_ds were assumed to be approximately normally distributed. The σ of these residuals was computed, and 95% of the prediction intervals were defined as $\pm 1.96\sigma$ around each prediction. This approach provides an interpretable measure of expected prediction error and reflects aleatory uncertainty arising from data variability. 2) Bootstrap uncertainty estimation was applied to quantify model stability and sensitivity to training data sampling. A total of 30 bootstrap resamples were generated from the training dataset, and a RF model was trained on each resampled dataset. Predictions from all bootstrap models were aggregated to compute the σ of predictions for each test sample, representing epistemic uncertainty associated with model structure and limited data availability. 3) Uncertainty calibration was evaluated using coverage probability analysis. The proportion of test observations falling within the estimated 95% of the prediction intervals was calculated to assess whether the uncertainty bounds were statistically meaningful and well calibrated. Coverage values close to the nominal confidence level indicate reliable uncertainty estimates and strengthen confidence in model deployment. In addition, feature importance analysis was conducted for all models built in feature ranking to identify the most influential HVSR parameters for f_d prediction. A rigorous validation framework was implemented to assess model performance and quantify prediction uncertainty. The dataset was partitioned using a 70–30 hold out split, with 30% reserved as an independent test set for final evaluation. Multiple performance metrics and uncertainty quantification methods were employed as detailed in Table 2.

Table 2 - Model evaluation metrics and uncertainty analysis methods applied to HVSR f_d prediction. In the formulas y_i represents the actual values, $\hat{y}_i$ the predicted values, $\bar{y}$ the mean of actual values, σ the standard deviation, B the 100 bootstrap iterations, T the number of trees, and $\Delta I_{t,j}$ the impurity decrease for feature j in tree t.

Category	Metric	Formula
Performance metrics	Root mean square error (*RMSE*)	$RMSE = \sqrt{\frac{1}{n}\sum_{i=1}^{n}\left(y_i - \hat{y}_i\right)^2}$
	Mean absolute error (*MAE*)	$MAE = \frac{1}{n}\sum_{i=1}^{n}\lvert y_i - \hat{y}_i \rvert)$
	Coefficient of determination (R^2)	$R^2 = 1 - \frac{\sum_{i=1}^{n}\left(y_i - \hat{y}_i\right)^2}{\sum_{i=1}^{n}\left(y_i - \bar{y}\right)^2}$
Uncertainty methods	Residual-based prediction intervals	$PI_{95\%} = \pm 1.96{*}\sigma_{res}$
	Bootstrap un uncertainty	$\sigma_{bootstrap} = \sqrt{\frac{1}{B-1}\sum_{b=1}^{B}((\hat{y}_b - \hat{y})^2}$
Feature analysis	Feature importance	$Importance_j = \frac{1}{T}\sum_{t=1}^{T}\Delta I_{t,j}$

The comprehensive evaluation included: 1) multi metric performance assessment on the independent test set; 2) three tier uncertainty quantifications using residual analysis, bootstrap sampling, and coverage probability; and 3) feature importance analysis to identify the most influential HVSR parameters. This integrated approach ensures reliable model assessment and provides practical uncertainty estimates for seismic site characterisation applications in data scarce regions.

Although the training was performed on Japanese data, the AutoHVSR framework is designed to be adaptable. The relationships learned, such as the link between the HVSR curve shape and f_d, are expected to hold under similar geological conditions, including those present in the Kathmandu Valley, which are characterised by thick, unconsolidated sediment layers, topographic basins, and urban exposure to seismic hazards. By establishing this methodology, a scalable and AutoHVSR analysis pipeline is provided and can be applied to regions with sparse seismic instrumentation. Future work will focus on integrating local microtremor recordings and geotechnical data from Kathmandu, further refining the model for region specific conditions. Ultimately, this approach supports improved seismic microzonation and vulnerability assessment in one of Nepal's most earthquake prone urban environments. All ML implementations were performed in MATLAB R2018a using built in functions with standardised preprocessing. Feature vectors were automatically z-score normalised before SVR training, while RR and RF models used the raw feature values as specified in their respective mathematical formulations.

2.5. Regional transferability evaluation

To evaluate whether HVSR features derived from the KiK-net database can be transferred to the Kathmandu Valley conditions, a feature space overlap assessment was performed. Distributions of f_d and peak amplification from Japanese sites were compared with the expected site response characteristics of the Kathmandu basin. For the Kathmandu Valley, the representative values of f_d and amplification ratio were taken from Poudyal *et al.* (2024). Since both regions consist of deep sedimentary deposits that typically resonate within the low to mid frequency range, this comparison provides a basis for assessing geological compatibility between the datasets. The observed overlap in the primary frequency band and amplification pattern shows that the Japanese recordings capture basin behaviour that is broadly similar to that of the Kathmandu Valley. This provides the quantitative justification for using KiK-net-based HVSR features as inputs to the ML models developed for site classification and microzonation.

3. Results

This section presents the comprehensive results obtained from the HVSR analysis and subsequent ML model implementations. The findings are derived from the KiK-net dataset comprising 2,363 earthquake recordings (2010–2025) and are organised to systematically evaluate: 1) the temporal variations in site response characteristics across Japanese seismic stations, 2) comparative performance of the three ML models in predicting f_d, 3) robust uncertainty quantification through multiple statistical approaches, and 4) identification of the most significant HVSR features controlling site response prediction. The primary objective of this analysis is to validate the accuracy of the AutoHVSR framework and reliability for f_d estimation, establishing its potential for transferability to data scarce regions like the Kathmandu Valley.

3.1. HVSR characteristics and temporal variations

The HVSR analysis reveals significant insights into site response characteristics across Japanese seismic stations. Fig. 2 presents the yearly distribution of HVSR curves from 2010 to 2025, generated using the KiK-net strong motion dataset. Each subplot illustrates the variability in spectral amplification across different seismic events and sites within a given year. While individual HVSR curves (in multiple colours) reveal diverse resonance characteristics, the bold red line represents the mean HVSR response for each year, highlighting consistent peak frequency trends.

The yearly mean HVSR plots from 2010 to 2025 demonstrate significant variability in

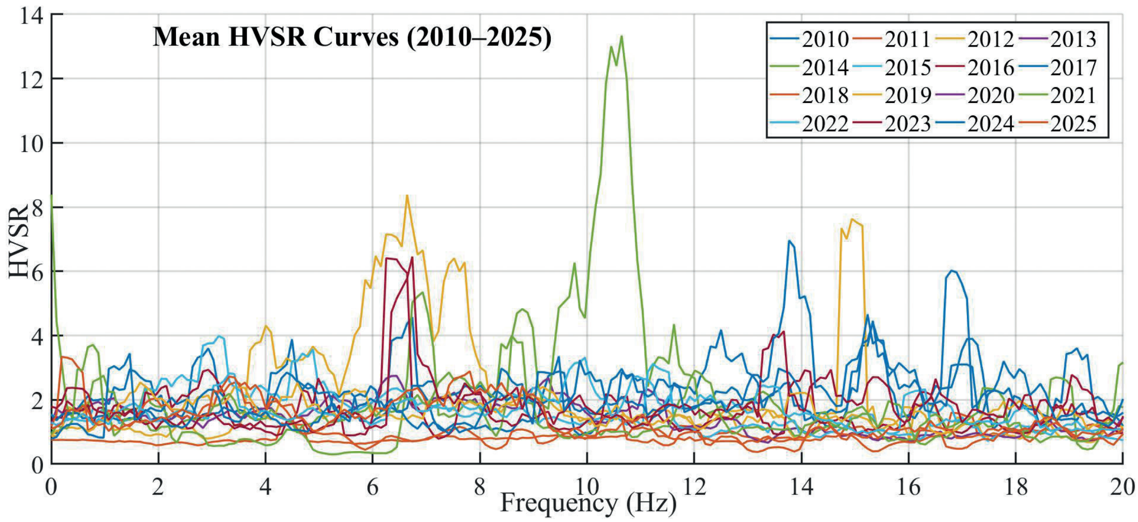

Fig. 2 - Yearly mean HVSR curves derived from KiK-net records from 2010 to 2025. Each curve represents the annual average HVSR computed from all available seismic recordings for the corresponding year.

amplification characteristics, reflecting diverse site conditions across Japan and offering valuable insights for future application in the Kathmandu Valley. The curves for 2010 and 2011 show moderate amplification with broad peaks, which is typical of relatively stiff soil profiles with low resonance concentration. By 2012 and 2013, several sharp peaks appear in the lower frequency range (5 to 15 Hz), indicating sites with thicker soft sediments that are more susceptible to ground motion amplification. This pattern continues in 2014 and 2015, with visible high amplitude peaks reaching above 20, typical of unconsolidated, deep alluvial deposits.

In contrast, the curves for 2016 and 2017 present more scattered spectral behaviour with relatively flatter responses, possibly representing mixed site conditions or stiffer geologic layers. The 2018 to 2020 period shows a return to prominent low frequency amplification patterns, suggesting a reappearance of soft soil site recordings, particularly in 2019, where sharp peaks at around 6–10 Hz dominate the mean response. The more recent years, 2021 to 2025, exhibit generally smoother mean HVSR curves, although isolated high peaks are still observed in individual sites, reflecting continued diversity in local site geology. These yearly variations in HVSR characteristics mirror the heterogeneity of subsoil conditions captured across the KiK-net and confirm the robustness of the feature extraction process used for training ML models. More importantly, such variations resemble conditions expected in the Kathmandu Valley, where unconsolidated sediment thicknesses vary spatially and influence amplification behaviour. By analysing how HVSR patterns evolve annually across diverse sites, this study builds a transferable knowledge base that can be applied to data scarce regions, like Kathmandu, for improved site classification and seismic risk reduction.

3.2. Model performance metric

Four ML models were trained and tested to predict the f_d from HVSR-based features. Their performance was evaluated using R^2, *RMSE*, and *MAE*. The comparison is shown in Fig. 3.

Across all metrics, the linear SVR model exhibits the highest predictive accuracy, characterised by the highest R^2 and the lowest *RMSE* and *MAE* values, while the remaining models show comparable but comparatively reduced performance. This multi-metric comparison highlights

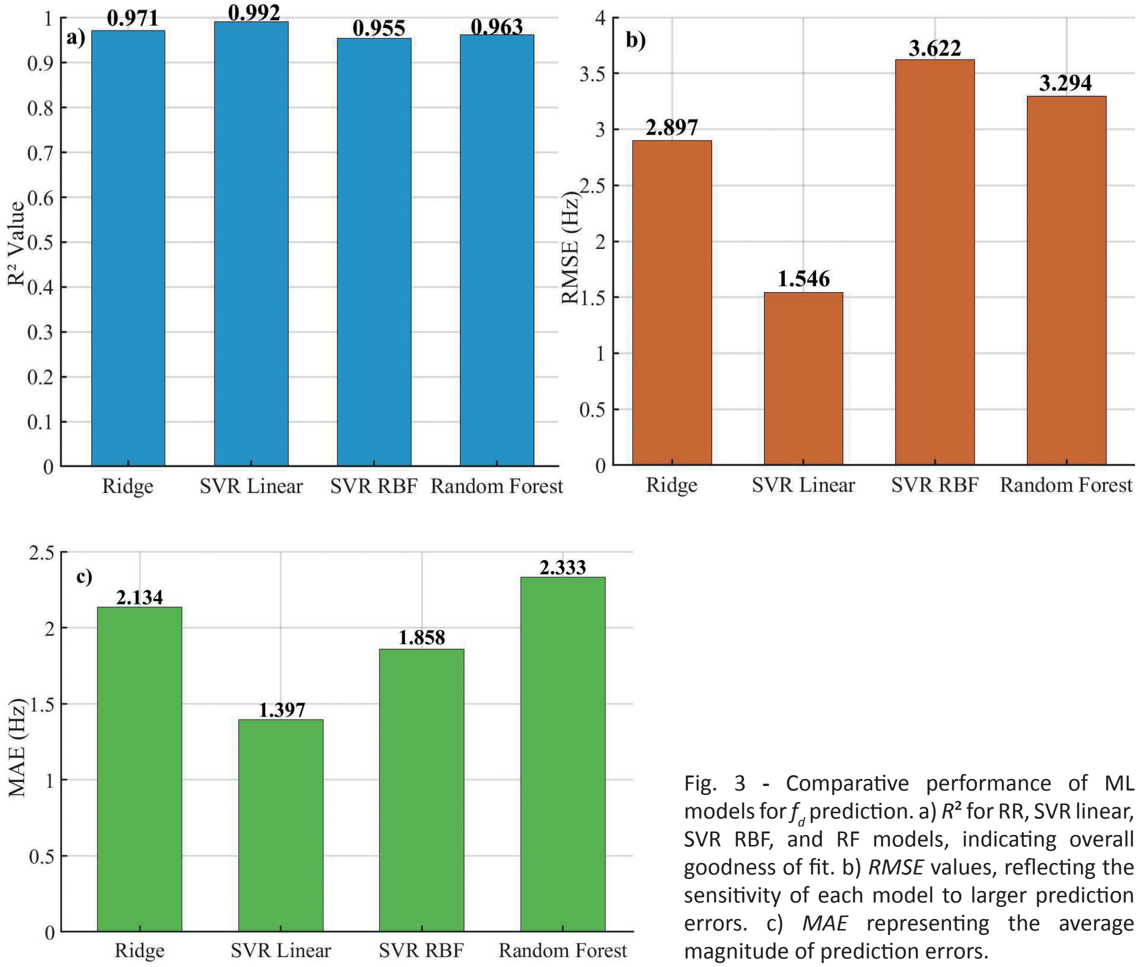

Fig. 3 - Comparative performance of ML models for f_d prediction. a) R^2 for RR, SVR linear, SVR RBF, and RF models, indicating overall goodness of fit. b) *RMSE* values, reflecting the sensitivity of each model to larger prediction errors. c) *MAE* representing the average magnitude of prediction errors.

the consistency of model ranking and supports the selection of linear SVR as the most reliable predictor within the evaluated framework. The linear SVR model gave the strongest performance across all metrics. It reached a R^2 of 0.992 (Fig. 3a), which means it explained nearly all of the variance in the test data. Its *RMSE* reached 1.546 Hz (Fig. 3b) and the *MAE* (1.397 Hz, Fig. 3c) was also the lowest among the four models, showing that its prediction errors were small and consistent. The RR model performed well but remained slightly behind the linear SVR model. Its R^2 was 0.971 and its errors were greater (*RMSE* 2.897 Hz, *MAE* 2.134 Hz). The predictions were stable but not as accurate as the linear SVR model. The SVR RBF model showed a mixed pattern. Even though its R^2 stayed reasonably high at 0.955, it produced the highest *RMSE* (3.622 Hz). This suggests that the NL kernel did not generalise well on this dataset and tended to produce larger deviations on some test samples. The RF model also reached a solid R^2 (0.963), but its *RMSE* (3.294 Hz) and *MAE* (2.333 Hz) were higher than both the linear SVR model and the RR model. This indicates that the ensemble model captured the general trend but was less precise at predicting exact f_d values. The scatter plot (Fig. 4) compares the actual f_ds with the values predicted by the four models. Most of the points from all models fall close to the 1:1 reference line, which shows that the models are able to capture the overall trend of the data.

The clustering of points along this line indicates the relationship between the input features and the site frequency. RR shows a tight alignment with the reference line across the full range, including the higher frequency values above 40 Hz, which suggests stable performance and low variance. Both SVR models perform consistently, although the linear version shows slightly more spread in the middle frequency range. The RBF version handles nonlinearity better, which is visible in its improved fit in the low to mid frequency range. RF tends to match the actual values well, but shows a few scattered points above 30 Hz. These outliers indicate that the model may slightly overfit or underfit in regions where data density is low.

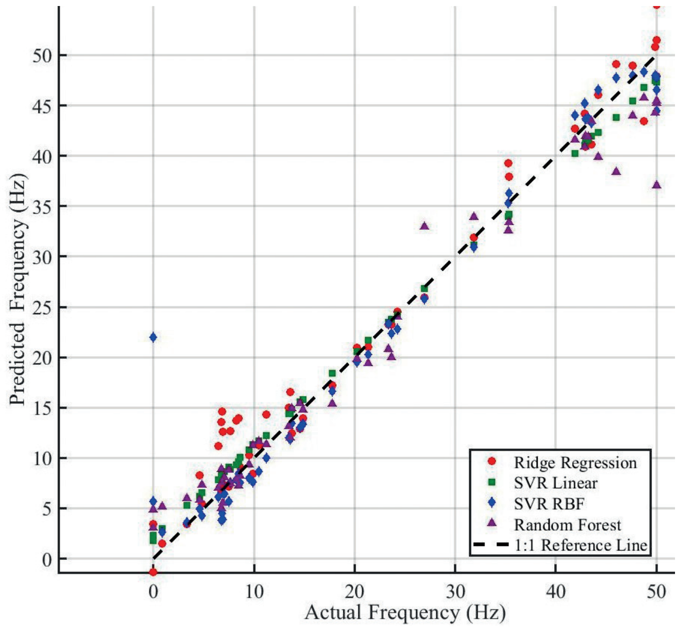

Fig. 4 - Actual versus predicted f_ds for the four models. Points clustered along the 1:1 reference line indicate good predictive alignment. RR and SVR RBF show the closest match to the ideal trend.

3.3. Uncertainty analysis

The residual histogram of the linear SVR model shown in Fig. 5 shows how well the predicted f_ds match the observed values.

Most of the residuals fall between about -2.5 Hz and +2.5 Hz, with a clear concentration on the negative side. This indicates that the model tends to slightly overpredict the frequency for many records. The distribution is not perfectly symmetric, but remains centred close to zero, which means the model does not show a strong systematic bias. A few larger positive residuals appear beyond +2 Hz, suggesting occasional underprediction for higher frequency sites. The overall spread of the residuals supports the *RMSE* and *MAE* values reported earlier and confirms that the linear SVR model provides stable predictions with moderate random error and limited extreme deviations.

Fig. 6 presents the comparison between the predicted and actual frequency values using a bootstrap-based model evaluation approach. The blue line represents the bootstrap mean predictions, while the green shaded region indicates the 95% confidence interval (CI), showing the uncertainty range of the predicted frequencies. The blue dots correspond to the actual observed frequency values for each sample.

The predicted frequencies closely follow the actual data trend, indicating that the model is capable of capturing the NL variability in frequency response with a high degree of accuracy. The narrow CIs for most samples suggest low prediction uncertainty and model stability. A

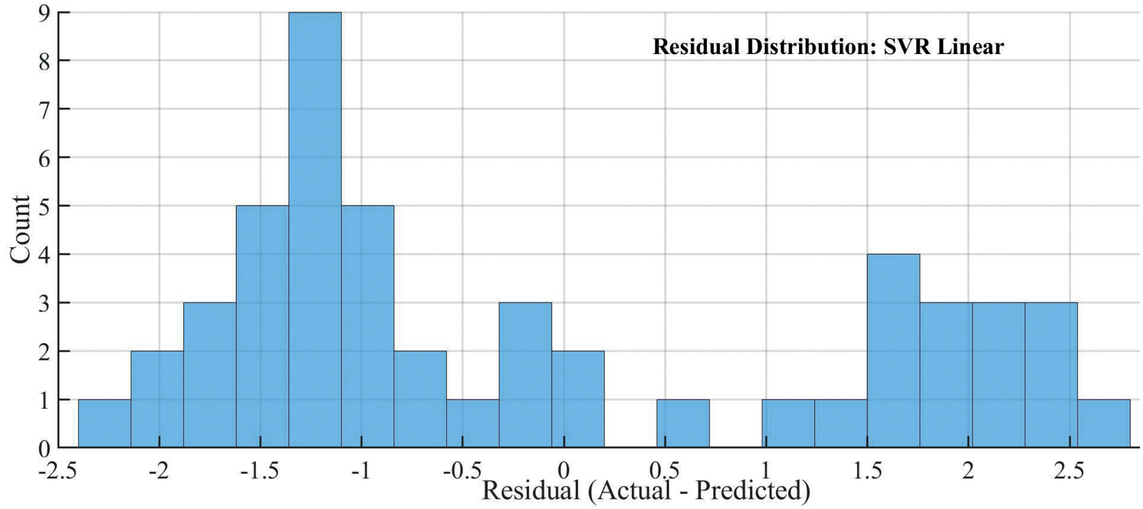

Fig. 5 - Residual distribution of the linear SVR model showing the difference between actual and predicted f_ds. Most residuals cluster near zero, indicating stable model performance with limited large errors.

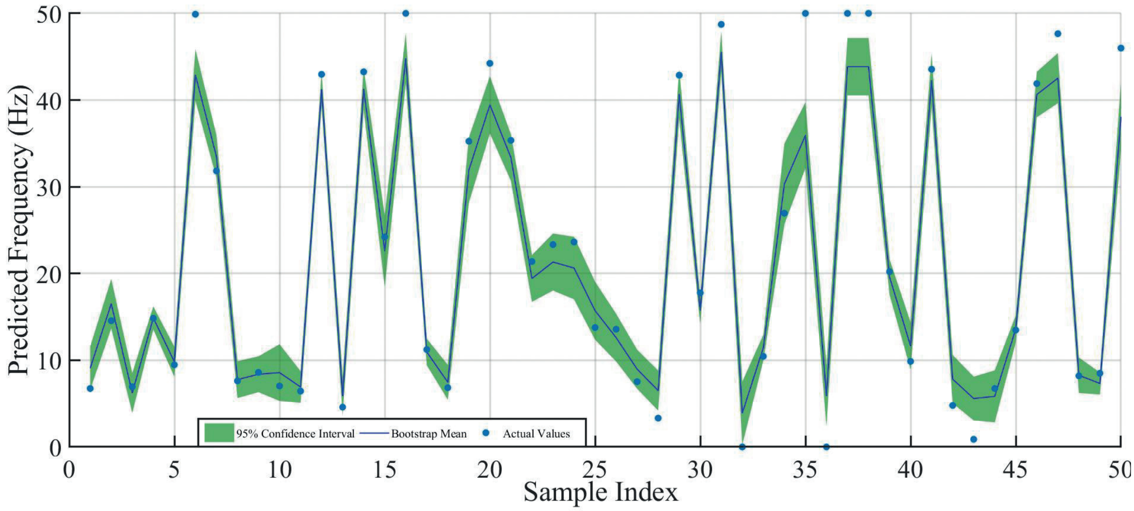

Fig. 6 - Comparison of predicted and actual frequencies using the bootstrap approach. The blue line represents the bootstrap mean, the green shaded area indicates the 95% CI, and the blue dots denote actual frequency values, showing strong agreement between model predictions and observed data.

few samples show relatively wider confidence bands, particularly at higher frequency ranges, implying greater variability or possible data sparsity in those zones. The close alignment between the bootstrap mean and actual values across the majority of samples demonstrates the robustness of the model in estimating frequency parameters. This consistency further supports the reliability of the employed prediction framework in modelling frequency dependent site response characteristics.

To further quantify model uncertainty, Fig. 7 illustrates a detailed comparison between residual-based and bootstrap-based uncertainty metrics. Fig. 7a shows the residual distribution, where most residuals are centred near zero, indicating that prediction errors are unbiased and

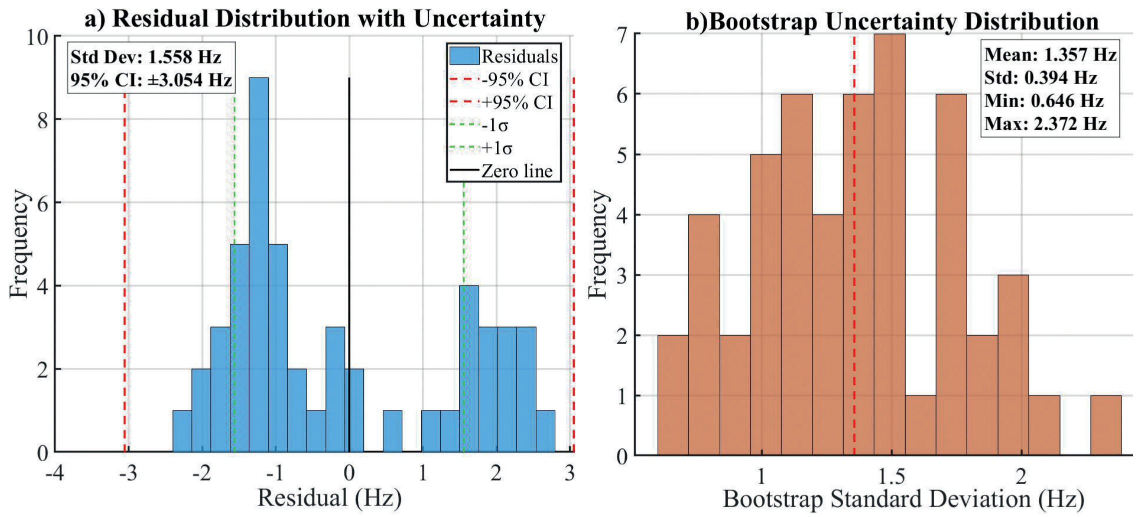

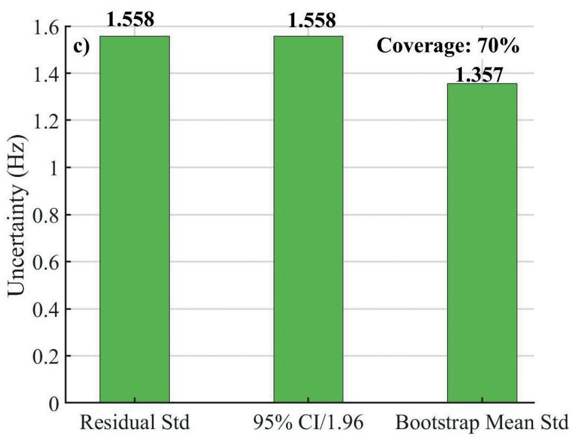

Fig. 7 - Residual-based and bootstrap-based uncertainty analysis of the linear SVR model. a) Residual distribution of predicted f_d, showing the zero reference line and the 95% CI, used to assess prediction bias and dispersion. The near zero centred residuals indicate the absence of systematic bias. b) Bootstrap-based uncertainty distribution of the residual σ, illustrating the stability of uncertainty estimates across resampled data subsets. c) Comparison of uncertainty metrics, including residual σ, normalised CI width (95% CI / 1.96), and bootstrap mean uncertainty, with overall coverage probability indicated.

well distributed. The residual σ of 1.558 Hz and a 95% CI of ±3.054 Hz confirm moderate variability with limited extreme deviations. Fig. 7b presents bootstrap uncertainty distribution, which estimates prediction variability through repeated resampling. The mean bootstrap uncertainty is 1.357 Hz with a σ of 0.394 Hz, suggesting consistent model performance across resamples. Fig. 7c compares multiple uncertainty indicator residual σ, 95% CI / 1.96, and bootstrap mean uncertainty showing strong agreement and a coverage rate of 70%. These results confirm that the linear SVR model captures prediction uncertainty effectively and provides stable, reliable estimates of the f_d.

3.4. Feature analysis

Fig. 8 illustrates the relative importance of input features, such as peak amplitude, peak frequency, mean amplitude, σ of amplitude, and mean frequency, across four ML models: RR, linear SVR, SVR RBF, and RF. The heatmap and bar plots clearly indicate that the peak frequency is the most dominant feature in all models, while the contributions of other parameters are minimal.

For the RR model, peak frequency (0.51) and mean frequency (0.43) exhibit comparatively higher importance, suggesting that frequency related parameters significantly influence model prediction. Mean amplitude (0.04) and σ of amplitude (0.02) show very low contributions, and peak amplitude is almost negligible. Similarly, both linear SVR and SVR RBF models highlight peak frequency as the most influential variable, with importance values of 0.98 and 0.91, respectively, while all other features contribute less than 0.1. This pattern indicates that variations in the f_d play a decisive role in determining the output of these models. The RF model shows a feature importance distribution nearly identical to RR, again emphasising peak frequency and mean frequency as key predictors.

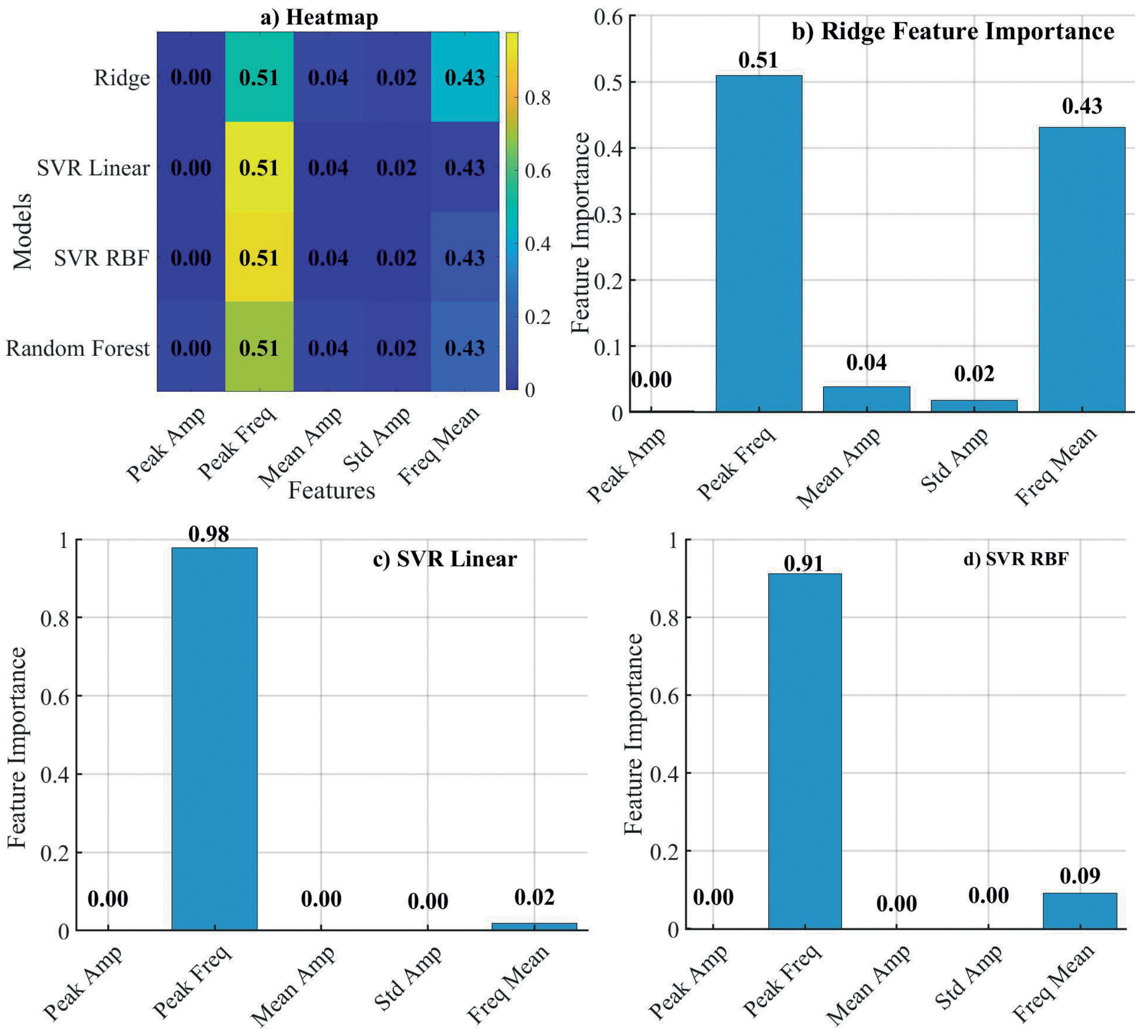

Fig. 8 - Feature importance comparison of RR, linear SVR, SVR RBF, and RF models. a) Heatmap of normalised feature importance values for RR, linear SVR, SVR RBF, and RF models, illustrating the relative contribution of each HVSR derived feature across algorithms. b) Feature importance obtained from the RR model, highlighting the role of peak frequency. c) Feature importance from the linear SVR model, showing a strong dependence on peak frequency with negligible contribution from amplitude-based parameters. d) Feature importance from the SVR RBF model, demonstrating a consistent importance pattern despite differences in model structure.

3.5. Regional transferability evaluation

The histograms (Fig. 9) show that the KiK-net dataset covers a wider and more continuous range of peak frequencies and peak amplifications compared to the values reported by Poudyal *et al.* (2004). In Fig. 9a, most of the KiK-net sites fall roughly between 1 and 12 Hz, with a dense concentration near the upper part of this range. The minimum and maximum values reported in the earlier Kathmandu Valley study lie inside this distribution but represent only a narrow portion of it. This indicates that the local study captured the primary basin response

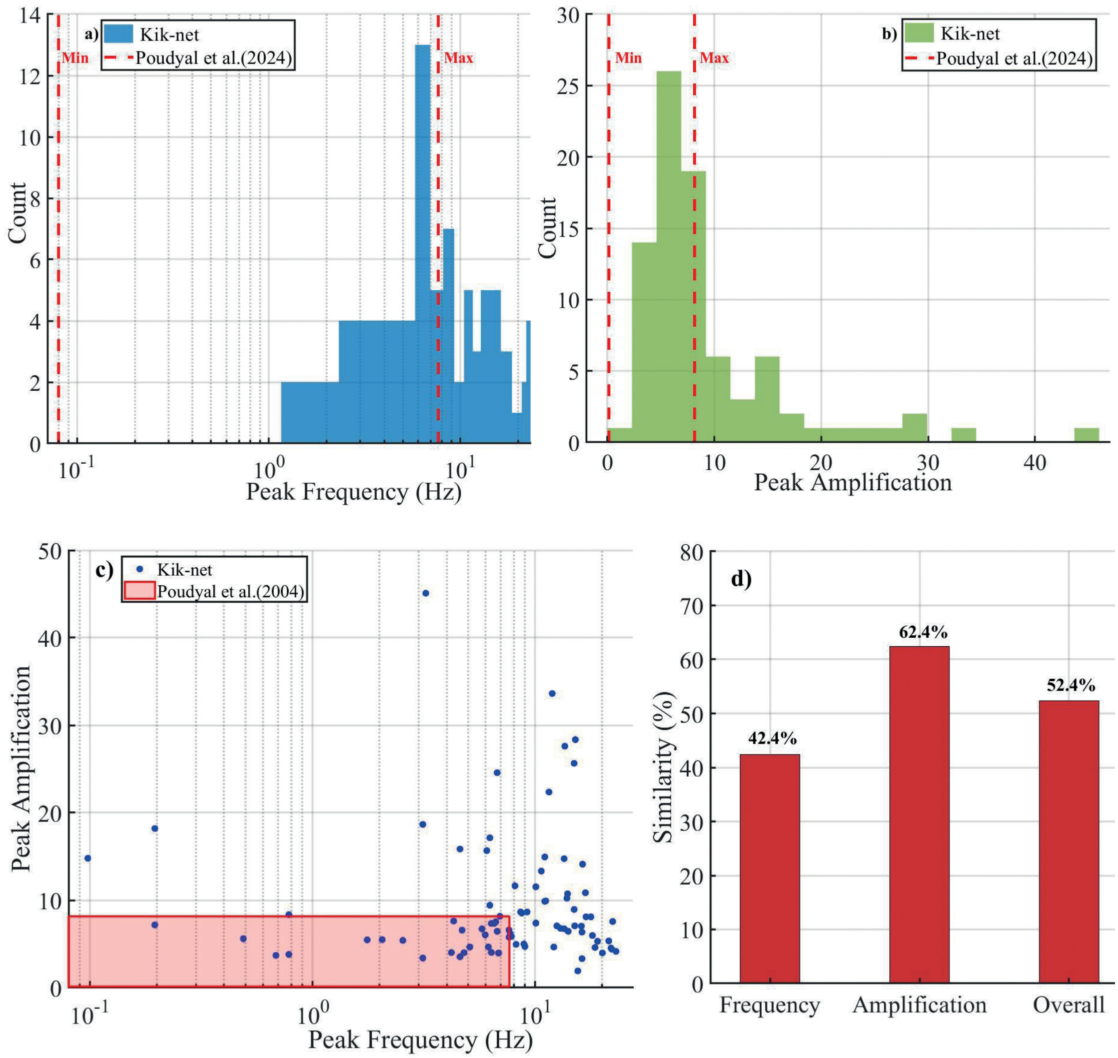

Fig. 9 - Feature space overlap between KiK-net HVSR characteristics and the expected site response range for the Kathmandu Valley. a) Histogram of f_d derived from the KiK-net database, with the minimum and maximum values reported for the Kathmandu Valley based on Poudyal *et al.* (2004) indicated by dashed lines. b) Histogram of peak amplification from the KiK-net, with the corresponding Kathmandu Valley range shown for reference. c) Joint distribution of peak frequency and peak amplification for KiK-net stations, overlaid with the expected Kathmandu Valley response envelope, illustrating the degree of overlap in the combined feature space. d) Quantitative similarity indices summarising the overlap for frequency, amplification, and their combined behaviour.

but did not sample the full variability that appears in a larger and more diverse strong motion dataset.

A similar pattern is evident in the amplification histogram (Fig. 9b). KiK-net values exhibit a long tail with amplifications exceeding 30, whereas the range from Poudyal *et al.* (2024) is comparatively short and located in the denser part of the distribution. This suggests that the earlier findings are consistent with the central tendency of KiK-net observations but do not represent the full range of potential amplification levels observed in deep or highly stratified sedimentary sites. The scatter plot (Fig. 9c) of peak amplification versus peak frequency reinforces this interpretation. KiK-net sites produce a cloud of points with substantial vertical spread, reflecting strong site-to-site differences in amplification even at similar frequencies. The rectangular region representing Poudyal *et al.* (2004) occupies a small, low amplification corner of the plot. This highlights that the Kathmandu Valley values fall within the KiK-net envelope but do not extend into the higher amplification domain, which is often associated with thicker or more NL sediment profiles. The similarity plot (Fig. 9d) provides a quantitative comparison between the two datasets. The frequency similarity of about 42.4% suggests moderate overlap, indicating that the f_ds reported for the Kathmandu Valley correspond to a subset of the broader KiK-net distribution. The amplification similarity of 62.4% is higher, showing that the Kathmandu Valley amplification levels align more closely with typical KiK-net behaviour. The overall similarity of 52.4 percent reflects partial agreement, consistent with the idea that the regional dataset captures the main response characteristics but lacks the diversity present in the larger Japanese database.

Although the ML models were trained using data from Japan, the geological characteristics of the Kathmandu Valley make this approach broadly transferable. The valley contains thick Quaternary sediments, complex basin geometry, and limited strong motion instrumentation, conditions that parallel many KiK-net sites. The feature space overlap assessment further shows that the f_d and amplification patterns occurring in Japanese sedimentary basins fall within the expected response range of the Kathmandu Valley. This suggests that the relationships learned from KiK-net, including the link between HVSR curve shape and peak frequency, remain valid for Kathmandu-like environments. The present results, therefore, provide a proof of concept, demonstrating that HVSR-based ML can support scalable site characterisation and microzonation in data scarce regions. In future work, the framework will be fine-tuned using locally collected microtremor or seismic data to capture region specific behaviour more accurately and enhance its applicability to the Kathmandu Valley.

4. Discussion

The comparative analysis of the developed ML models demonstrates that the framework effectively captures the relationship between HVSR-derived features and the site f_d. The close clustering of predicted and observed frequencies along the 1:1 reference line confirms the robustness and reliability of the models. The linear SVR model, in particular, exhibited the highest predictive accuracy with a R^2 of 0.992 and the lowest *RMSE* and *MAE* values, indicating that the frequency–feature relationship in this dataset is predominantly linear. RR also performed consistently, though with slightly higher prediction errors, while RF and SVR RBF models showed moderate deviations at the extremes of the frequency range. These differences suggest that, while NL and ensemble approaches can capture complex variability, the linear mapping between frequency and HVSR parameters remains dominant for the studied dataset. The selected performance metrics were chosen to reflect both statistical accuracy and practical applicability of the proposed workflow. *RMSE* provides a direct measure of prediction error in physical units, which is particularly important for seismic site characterisation where absolute errors can influence ground motion estimates and design decisions. The R^2 complements this by indicating how well the model captures spatial and site-specific variability in amplification characteristics. Together, these metrics enable the assessment not only of the predictive accuracy but also of the reliability of the model for real-world deployment, especially in data-scarce regions where robust and interpretable performance measures are essential.

The residual-based and bootstrap-based uncertainty analyses further confirm the model's stability. Most residuals clustered near zero, indicating minimal systematic bias, while the narrow 95% CIs highlight low uncertainty and consistent performance across samples. Minor deviations at higher frequency values likely arise from sparse data distribution and variations in site specific soil conditions, particularly at sites with stiffer or thinner sedimentary layers. Despite these variations, the predictive reliability of the model remained strong, demonstrating its potential applicability beyond the original KiK-net dataset.

The feature importance evaluation provides valuable insights into the physical meaning behind the model performance. Across all four models, peak frequency consistently emerged as the most influential feature, followed by mean frequency, while amplitude related parameters contributed marginally. This dominance of frequency parameters underscores their fundamental role in representing site stiffness and resonance characteristics, aligning with established seismological understanding. The results validate that frequency domain features derived from HVSR analysis carry the most critical information for predicting site response behaviour. Beyond standard performance metrics, statistical robustness was evaluated through multimodel consistency, uncertainty calibration, and feature dominance analysis across a large number of stations and recording years. The convergence of model performance metrics, stable residual distributions, and consistent feature importance rankings across different learning algorithms indicates that the learned relationships are not site specific artefacts but reflect general site response behaviour captured within the KiK-net. This internal statistical consistency provides indirect but meaningful evidence supporting the methodological transferability of the proposed framework. Nevertheless, full confirmation of regional generalisability requires validation using independent datasets from geologically distinct areas, which is identified as an important direction for future work.

The overall consistency of the findings shows that the proposed ML framework can function as a dependable predictive tool for site classification and seismic microzonation. The ability of the model to learn stable relationships from the KiK-net database suggests its potential for transferability to other tectonically active basins. For the Kathmandu Valley, where deep sediment deposits and basin geometry resemble conditions at several KiK-net sites, the framework offers a practical approach for regions with limited ground motion records. By connecting HVSR derived spectral features to f_d through interpretable ML models, this study outlines a scalable path for estimating regional site response and supporting improved seismic hazard mapping in the central Himalayas.

The use of HVSR-based features also strengthens the applicability of the model beyond Japan, since the predictive variables reflect physical soil properties rather than region specific characteristics. Parameters such as peak and mean frequency primarily capture impedance contrast and sediment stiffness, which follow similar trends across many sedimentary basins. Previous studies report that the Kathmandu Valley exhibits site periods and amplification levels that fall within the feature ranges observed in the KiK-net, further supporting the model suitability for Nepalese conditions. This alignment indicates that the framework can operate reliably in Kathmandu, provided that local sites share comparable frequency domain characteristics.

The results align with the broader pattern reported in earlier studies that combined HVSR analysis with ML. Previous studies showed that HVSR features contain enough structure for ML models to extract reliable information about site behaviour, whether the goal is automated peak picking, site classification, or amplification prediction. The strong performance of the linear SVR model in this study supports such trend. It shows that f_d can be predicted with consistent accuracy using a small set of HVSR-derived features, similar to how earlier studies used HVSR to classify sites or estimate amplification. The finding that frequency related parameters carry most of the predictive weight is also consistent with the AutoHVSR results reported by Vantassel *et al.* (2023) and with the feature importance patterns observed in more complex models such as those used by Wang *et al.* (2023). While this study focuses on f_d rather than amplification or site class, the overall behaviour of the model fits well within the growing body of evidence that ML provides stable and interpretable improvements in HVSR-based site characterisation.

While the results are promising, several limitations should be noted. The dataset contains 1,654 samples, which is less than the datasets used in earlier large scale studies. A limited dataset can restrict the range of soil profiles represented and may reduce the model ability to recognise rare or extreme site conditions. Another limitation is the regional focus of the data. All records originate from Japan, and although many KiK-net sites resemble sedimentary basins found in the Kathmandu Valley, regional bias may still influence the learned relationships. The final limitation is the reliance on standard algorithms such as SVR, RR, and RF. These methods work well but do not use domain specific constraints or recent advances in transfer learning that may improve cross regional applicability.

To directly address these limitations and advance the development of robust, globally applicable site-response models, we propose a multi-faceted strategy for future work:

1. cross-regional validation and benchmarking. A critical next step is systematic validation against datasets from diverse tectonic and geological settings (e.g. Taiwan, Italy, California, and, specifically, the Kathmandu Valley). We recommend a phased validation strategy, beginning with geologically analogous regions before testing in contrasting settings. Establishing open benchmark datasets and standardised evaluation protocols would enable objective comparison across studies and help quantify regional biases;
2. data integration and feature enhancement. To mitigate regional bias and improve generalisability, future models should integrate publicly available global data from networks like Center for Engineering Strong Motion Data and NGA-West2. Concurrently, expanding the feature set to include parameters such as V_{s30}, resonance frequency bandwidth, or morphological indicators of the HVSR curve shape could capture a broader spectrum of site variability;
3. advanced modelling techniques. These move beyond standard algorithms, thus propose exploration;
4. domain adaptation and transfer learning. A model pre-trained on the large Japanese dataset can be fine-tuned with a smaller set of local recordings (e.g. from microtremor arrays in the Kathmandu Valley). This bridges regional differences without requiring extensive local data;
5. physics-informed or hybrid models. These incorporate domain knowledge through

physics-guided neural networks or hybrid ensembles which can regularise learning, improve extrapolation, and model NL site effects more effectively than purely data-driven approaches;
6. sensitivity and uncertainty quantification. Conducting sensitivity analyses will be crucial to understand how regional differences in key parameters (e.g. soil stiffness profiles, impedance contrasts) affect model performance. This should be coupled with enhanced uncertainty quantification to provide more reliable probabilistic inputs for seismic hazard assessment.

By pursuing these concrete steps, validation, data diversity, advanced algorithms, and rigorous uncertainty analysis of future work can transform the current workflow into a more powerful, generalisable, and trustworthy tool. This will significantly improve site-specific seismic hazard assessments, particularly in data limited regions that stand to benefit the most from robust transferable models.

5. Conclusions

This research demonstrates the successful integration of the AutoHVSR framework with ML techniques for seismic site characterisation, using a comprehensive dataset from the Japan KiK-net. The yearly HVSR analysis revealed clear temporal and spatial variations in site amplification behaviour, linked to subsurface geological diversity. ML models trained on HVSR-derived features, particularly f_d-related parameters, showed consistently high predictive performance, with the linear SVR model yielding the most stable results. These findings suggest that f_d can be efficiently estimated from HVSR spectral features using interpretable and computationally efficient models. Compared to traditional manual HVSR processing, the proposed automated workflow primarily contributes by improving consistency, reducing subjectivity, and enabling reproducible large scale analyses, rather than replacing established site characterisation approaches. The feature space overlap analysis indicates that the range of f_ds and amplification characteristics observed in KiK-net data overlaps with those expected for sedimentary basins such as the Kathmandu Valley. This observation supports the physical relevance of the learned relationships, while acknowledging that direct validation using local data remains necessary.

Acknowledgments. The datasets supporting the findings of this study are freely available online and can be downloaded from https://www.kyoshin.bosai.go.jp/en. The author used ChatGPT by OpenAI to assist with paraphrasing and improving the readability of the manuscript. All content generated was thoroughly reviewed and revised by the author, who takes full responsibility for the final version of the manuscript.

REFERENCES

Cai J. and Xi N.; 2024: *Site classification methodology using support vector machine: a study*. Earthquake Res. Adv., 4, 100294, doi: 10.1016/j.eqrea.2024.100294.

Dhakal Y.P., Kubo H., Suzuki W., Kunugi T., Aoi S. and Fujiwara H.; 2016: *Analysis of strong ground motions and site effects at Kantipath, Kathmandu, from 2015 Mw 7.8 Gorkha, Nepal, earthquake and its aftershocks*. Earth Planets Space, 68, 1-12, doi: 10.1186/s40623-016-0432-2.

Lachet C. and Bard P.Y.; 1994: *Numerical and theoretical investigations on the possibilities and limitations of Nakamura's technique*. J. Phys. Earth, 42, 377-397, doi: 10.4294/jpe1952.42.377.

Nakamura Y.; 1989: *A Method for dynamic characteristics estimation of subsurface using microtremor on the ground surface.* Q. Rep. RTRI (railw. Tech. Res. Institute), 30, 25-33.

Nogoshi M. and Igarashi T.; 1971: *On the amplitude characteristics of microtremor (Part 2)*. J. Seismol. Soc. Japan, 24, 26-40, doi: 10.4294/zisin1948.24.1_26.

Nurwidyanto M.I., Zainuri M., Wirasatriya A. and Yulianto G.; 2023: *Microzonation for earthquake hazards with hvsr microtremor method in the coastal areas of Semarang, Indonesia*. Geogr. Tech., 18, 177-188, doi: 10.21163/GT_2023.181.13.

Phi F.G., Cho B., Kim J., Cho H., Choo Y.W., Kim D. and Kim I.; 2024: *Machine learning application to seismic site classification prediction model using Horizontal-to-Vertical Spectral Ratio (HVSR) of strong-ground motions*. Geomech. Eng., 37, 539-554, doi: 10.12989/gae.2024.37.6.539.

Pokhrel R.M., Gilder C.E.L., Vardanega P.J., De Luca F., Werner M.J. and Maskey P.N.; 2019: *Estimation of V S30 by the HVSr method at a site in the Kathmandu Valley, Nepal*. In: 2nd International Conference on Earthquake Engineering and Post Disaster Reconstruction Planning, Bhaktapur, Nepal, pp. 52-60.

Poudyal D., Roslan S.N.A. and Dahal B.K.; 2022: *Seismic microzonation of Kathmandu Valley: a review.* In: Proc., Bicer A., Akman O. and Unal M. (eds), International Conference on Engineering, Science and Technology (IConEST), Austin, TX, USA, Vol. IV, pp. 85-89.

Poudyal D., Nordin N., Roslan S.N.A. and Dahal B.K.; 2024: *Spatial mapping of seismic vulnerability index in Kathmandu Valley: insight from dominant frequency and amplification factor*. J. Geophys. Eng., 21, 1272-1285, doi: 10.1093/jge/gxae069.

Poudyal D., Banjade C., Dahal A., Shah A.K. and Yadav M.K.; 2025: *Machine learning and its integration with nonlinear ground response analysis in Bhaktapur District.* Nepal: Geomech. Geoengin., doi: 10.1080/17486025.2025.2596759.

Poudyal D., Nordin N. and Roslan S.N.A.; 2025a: *Comparative declustering approaches for seismic data: insights from Gardner Knopoff , Gruenthal , Reasenberg , and Uhrhammer in the Kathmandu Valley.* Ann. Geophys., 68, 1-23, doi: 10.4401/ag-9178.

Poudyal D., Nordin N. and Roslan S.N.A.; 2025b: *Estimation and mapping of Arias intensity in Nepal: Insights from seismic analysis in the Kathmandu Valley.* Contrib. to Geophys. Geod., 55, 31-47, doi: 10.31577/congeo.2025.55.1.3.

Poudyal D., Nordin N. and Roslan S.N.A.; 2025c: *Integrated earthquake risk assessment using PSHA-based microzonation and soil vulnerability index maps of urban Kathmandu Valley.* Ann. Geophys., 68, 1-15, doi: 10.4401/ag-9246.

Poudyal D., Nordin N. and Roslan S.N.; 2026: *A comparative statistical analysis of equivalent linear and nonlinear site response in the Kathmandu Valley, Nepal*: Bull. Geoph. Ocean., 67, 1-18, doi: 10.4430/bgo00504.

Saputra F.R.T., Rosid M.S., Fachruddin I., Ali S., Huda S. and Wiguna I.P.A.P.; 2022: *Analysis of soil dynamics and seismic vulnerability in Kalibening District, Banjarnegara using the HVSR method*. J. Phys. Conf. Ser., 2377, 012038, doi: 10.1088/1742-6596/2377/1/012038.

Supriyadi S., Muttaqin W.H., Khumaedi K. and Sugiyanto S.; 2022: *Soil vulnerability levels based on microtremor data using the HVSR method in the old city area of Semarang*. J. Phys. Theor. Appl., 6, 34, doi: 10.20961/jphystheor-appl.v6i1.59119.

Tiwari R.K., Poudel R.P. and Paudyal H.; 2025: *Machine learning for predicting earthquake magnitudes in the central Himalaya*. Bibechana, 22, 22-29, doi: 10.3126/bibechana.v22i1.70637.

Vantassel J.P., Stolte A.C., Wotherspoon L.M. and Cox B.R.; 2023: *AutoHVSR: a machine-learning-supported algorithm for the fully-automated processing of horizontal-to-vertical spectral ratio measurements*. Soil Dyn. Earthquake Eng., 173, 108153, doi: 10.1016/j.soildyn.2023.108153.

Wang X., Wang Z., Wang J., Miao P., Dang H. and Li Z.; 2023: *Machine learning based ground motion site amplification prediction*. Front. Earth Sci., 11, 1053085, doi: 10.3389/feart.2023.1053085.

Xu R. and Wang L.; 2021: *The horizontal-to-vertical spectral ratio and its applications*. EURASIP J. Adv. Signal Process., 2021, 75, doi: 10.1186/s13634-021-00765-z.

Zhu C., Cotton F., Kawase H., Eeri M. and Nakano K.; 2023: *How well can we predict earthquake site response so far? Machine learning vs physics-based modeling*. Earthquake Spectra, 39, 478-504, doi: 10.1177/87552930221116399.

Corresponding author: Dibyashree Poudyal Lohani
Department of Civil Engineering, Nepal Engineering College
Changunarayan Bhaktapur, Nepal
Phone +9779840090607; e-mail: dibyashreel@nec.edu.np